## Influence of subsurface microstructure variations on bending ductility of Aural™-2 HPVDC thin-walled components

Tremblay, X.; Gariépy, A.; Javidani, M.



*Proceedings of the 2024 North American Die Casting Association Congress & Exposition, 2024-10-02*

2024 DIE CASTING CONGRESS & EXPOSITION
NADCA
NORTH AMERICAN DIE CASTING ASSOCIATION



# Influence of Subsurface Microstructure Variations on Bending Ductility of Aural™-2 HPVDC Thin-Walled Components

**X. Tremblay**
Department of Applied Science, University of Quebec at Chicoutimi, Saguenay, Canada

**A. Gariépy[1] & M. Javidani[2]**
[1]National Research Council Canada, Saguenay, Canada
[2]Department of Applied Science, University of Quebec at Chicoutimi, Saguenay, Canada

## ABSTRACT

High pressure die casting is widely employed in the automobile industry for its ability to mass produce intricate aluminium parts, including sizable structural components made of specialized alloys. However, the size and complexity of the castings, combined with the current understanding of the rapid solidification process, can limit our control over the microstructure. More specifically, the fast turbulent flow of material during filling leads to the formation of distinct subsurface microstructure variants, often visible within one casting. Given that bending ductility is generally a key performance indicator for high-integrity castings, and is expected to be largely influenced by near-surface microstructure, this paper aims to characterize the observed microstructure variations in die cast aluminum specimens and assess their impact on local bending behaviour. The microstructure variations were characterized using optical microscopy on representative specimens, revealing distinct types of subsurface microstructure variants. Samples from region expected to present different types of subsurface microstructure variants underwent VDA bending tests. Mechanical testing demonstrated that these subsurface variants influence the bending behaviour. Considering these results, a deeper understanding of the mechanisms involved in the filling process could improve die design practices. Furthermore, this knowledge could facilitate the control of microstructure formation and enhance the overall homogeneity of mechanical performances throughout HPVDC components.

## INTRODUCTION

High pressure die casting (HPDC) is a widely used process for manufacturing aluminum products, especially automotive components made from Al-Si based alloys [1, 2]. The solidification of Al alloys in HPDC often results in an uneven dispersion of alloying elements, creating a wide range of microstructural compositions within a single component. Furthermore, the material flow during the HPDC process produces a layered microstructure typically composed of three regions: the core, the segregation bands, and the skin layer. These regions can generally be distinguished by the distribution of their main constituents. In structural applications, this heterogeneous structure controls the mechanical properties of the components [3-6].

The microstructure of structural hypoeutectic Al-Si based alloys has been widely investigated in the literature. The main constituents are generally the externally solidified crystals (ESCs), the primary aluminium phase (α-Al) and the eutectic. The primary aluminium phase (α-Al) and eutectic constituents solidify inside the die cavity, but the ESCs solidify while the material is still in the shot sleeve, prior to injection. As a result of the condition in the shot sleeve, ESCs solidify as larger dendritic crystals that can either remelt or get fragmented during the injection phase, hence their wide range of shapes and sizes [7].

Regarding the distinction between the regions, the core lies between the segregation bands and is generally characterized by a coarser α-Al phase and a high area fraction of ESCs, resulting in the lowest proportion of eutectic in the microstructure. In contrast, the skin layer consists of a finer primary phase and a low area fraction of ESCs, resulting in a relatively higher eutectic proportion [8]. Additionally, while the edge of the skin layer is not clearly defined, it is generally considered to be the zone between the segregation band and the die interface [9-11].

Segregation bands are thin, discontinuous regions of interconnected eutectic pockets that follow the part's contour parallel to the material flow direction. These bands of positive segregation are believed to result from dilatant shear banding that develops between cohesive solid networks during the pressure intensification phase of the process. The strain applied to the developing solid networks creates localized changes in solid packing density, promoting dilatant shear banding and, consequently, the segregation of solute-rich liquid in interconnected pockets between high solid fraction areas [8,12,13]. Segregation bands are generally more prominent in relatively thick sections, and are not always significant in thin-walled die castings. Furthermore, the accumulation of ESCs in the core region, combined with the high-speed material flow, have been identified as the most influential factors affecting the development, position, and thickness of the segregation bands [13,14].

The description and mechanisms involved in the near-surface microstructure formation have not been studied as extensively. It is already documented that the sub-surface can exhibit a range of characteristic microstructures, and these sub-surface microstructure variations have been related to the impingement level of the flow of material with the die interface, the development of dilatant shear banding, and pressure effects [9,10]. The local level of impingement influences the likeliness for solidification to start at the interface and the dilatant shear bending affect the segregation of solute rich liquid towards the surface during solidification.

One common requirement in structural castings, for crashworthiness and self-piercing riveting capability, is bendability as evaluated for instance by the VDA bend test [15]. As this test concentrates the strain on the surface, it appears likely that the skin layer could play a critical role on this aspect of service performance.

This paper therefore aims to identify the extent to which microstructure variations in HPDC thin-walled components could affect bending ductility homogeneity. Specifically, the experimental work aims to characterize microstructure variations in a simple prototype casting based on the distribution of the main constituents within the plate, with a focus on the skin layer, to correlate bending performance with local microstructure characteristics.

## MATERIALS AND METHODS

The high-pressure vacuum die casting (HPVDC) specimens studied in this experiment are 3 mm thick plates as illustrated in *Figure 1*. The specimens were produced with the Aural™-2 alloy, whose composition range is presented in *Table 1*. The material was a mix of primary ingots and in-process scrap (runners and overflows). All specimens were tested in the F-temper. The specimens were produced using a 530-ton Bühler SC N/53 cold-chamber die casting machine at the National Research Council Canada. This cell is equipped with automated metal ladling, spray functions, and a Fondarex vacuum system. Prior to the experiments, the material was melted in an electrically heated crucible furnace and treated with a Wedron metal treatment system for fluxing. Degassing of the melt prior to casting was ensured by argon injection. During the trials, the die face was operating at approximately 250-260°C and a relatively low amount of die lubricant was applied. More details on the experimental trials can be found in a prior paper [16]. All of the castings investigated herein were produced in nominally similar process conditions.

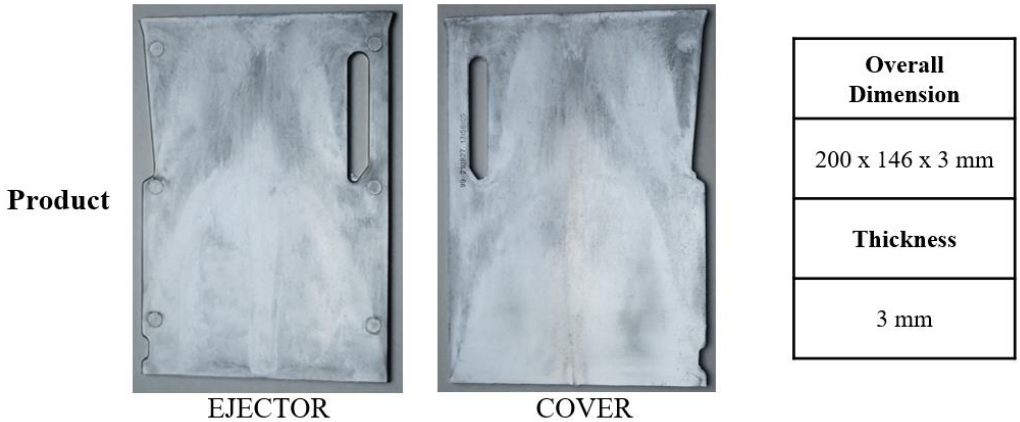


***Figure 1- HPVDC products characterized in this project.***

*Table 1- Aural™-2 alloy composition.*

| Element | Al | Si | Mg | Fe | Mn | Ti | Sr |
|---|---|---|---|---|---|---|---|
| wt. % | Bal. | 10.3-10.9 | 0.29-0.32 | 0.18-0.20 | 0.48-0.51 | 0.06 | 0.010-0.016 |

## MICROSTRUCTURE CHARACTERIZATION METHOD

The as-cast plates were sectioned into multiple samples for metallographic analysis. These samples were taken from areas near the gate, center, and overflow zones (*Figure 2*). All samples were then subjected to standard grinding and polishing procedures. Initially, they were ground with 6µm and 3µm diamond paste for 5 minutes each. This was followed by a final polishing step using 0.5µm colloidal silica for an additional 5 minutes.

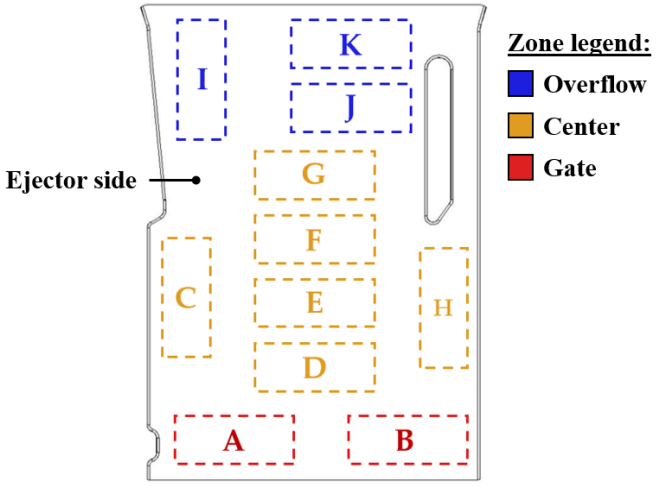


***Figure 2- Sample positioning on the HPVDC plate: A and B for the gate zone, C to H for the center zone, and I to K cover the overflow zone.***

As-polished samples from five plates were used for the microscopy analysis conducted in this study. The through-thickness microstructure was captured from the samples' cross-sections using 350x200 µm images, spanning from the ejector to the cover surface (*Figure 3(a)*). Additionally, the sub-surface microstructure was captured with 350x20 µm images, extending up to 300 µm from the surface (*Figure 3(b)*).

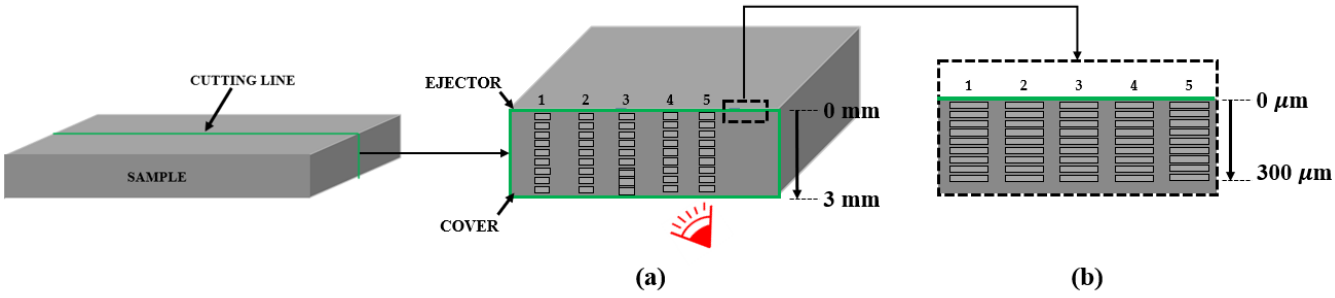


***Figure 3- Sampling and analysis methodology for the calculation of the main constituents' distribution: (a) through the plate's thickness and (b) in the first 300 µm from the surface.***

A Nikon Eclipse ME600 optical microscope was used to acquire the micrographs. Subsequently, a Clemex® image analysis routine was employed to segment the microstructure based on grayscale threshold analysis and calculate the area fraction of the main constituents (α-Al, eutectic, and ESCs). Intermetallics were not specifically quantified herein. This routine also calculates the average crystal area for the primary aluminum phase (α-Al) and the externally solidified crystals (ESCs) with a subjective threshold at 200 $\mu m^2$ to separate the two populations. For both the through-thickness and sub-surface characterizations, at least five locations per sample were analyzed for statistical sampling. The objective of this analysis was to assess the change in microstructure composition between the core and the skin layer, as well as the local variations at the die interface (sub-surface).

### BENDING PERFORMANCE EVALUATION METHOD

The bending performance was evaluated in accordance with the VDA 238-100 Tight Radius Bend Test using an MTS RT100 mechanical testing machine and a VDA test fixture from Zwick/Roell (*Figure 4*). The bend test specifications included a nominal punch radius of 0.4 mm and a roller gap of 6.8 mm, which remained consistent across all tests.

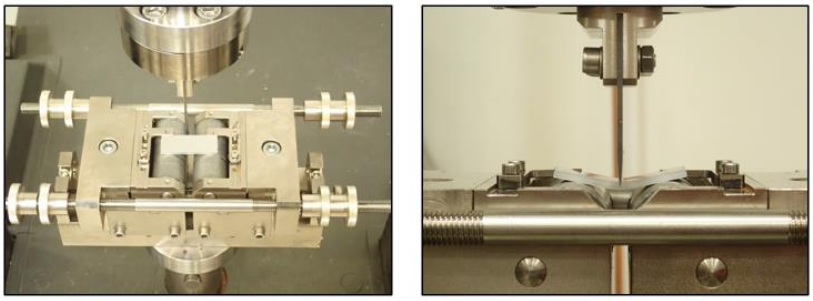

***Figure 4- VDA bending test set-up***

The samples used in this experiment were 20x50x3 mm in size and were machined based on the sample locations outlined in *Figure 2*. In total, twelve plates were machined. On each plate, specimens were tested for both the ejector and cover faces.

Following the bending test, the bent samples underwent preparation for optical microscopy using the previously outlined methodology. This analysis aims to establish a correlation between the sub-surface microstructure and the bending performance of each of the samples. Therefore, particular focus was placed on analyzing the distribution of constituents within the first 300 µm from the surface in the bending samples, close to the fracture location.

## RESULTS AND DISCUSSION

### GENERAL MICROSTRUCTURE CHARACTERIZATION

*Figure 5(a)* show a representative example of the microstructure obtained by HPVDC, where the characteristic regions of the layered microstructure are visible (core, segregation band and skin layer). As illustrated in *Figure 5(b)*, all the main constituents are easily distinguishable: the externally solidified crystals (ESCs), the primary aluminium phase (α-Al) and the eutectic. Given the simplicity of the specimen, constant thickness and use of vacuum, porosity amount remained very small and was not specifically analyzed herein.

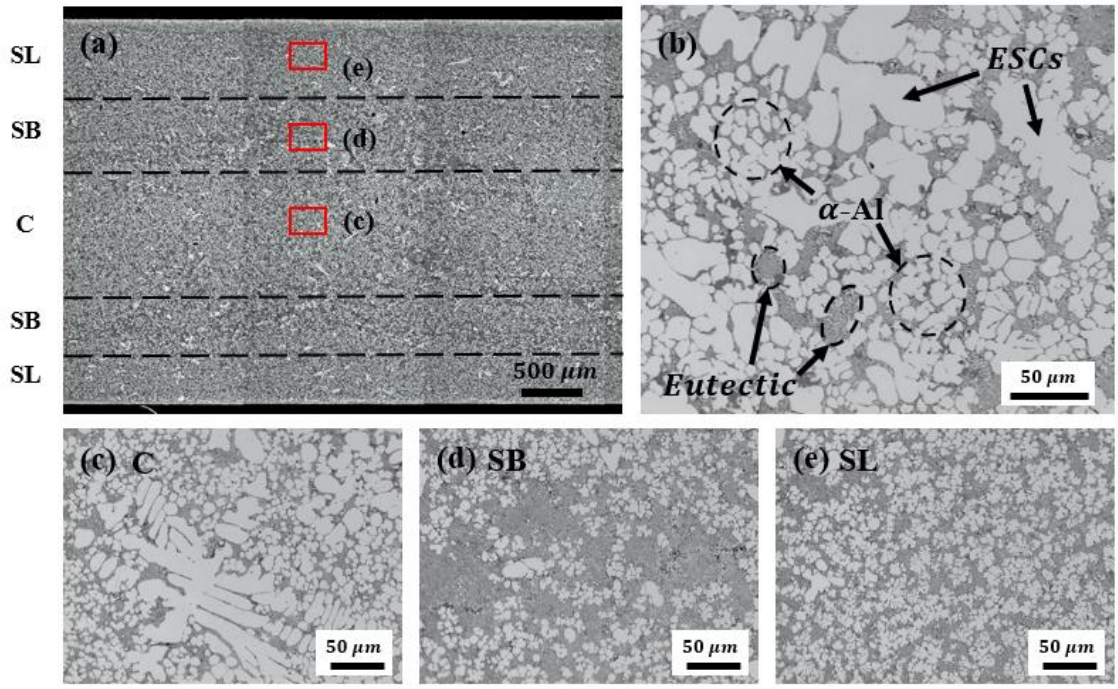


***Figure 5- Representative as-cast microstructure of the HPVDC Aural™-2 plate: (a)The through-thickness microstructure, (b) identification of the main constituents, (c) The core (C), (d) The segregation band (SB), and (e) the skin layer (SL).***

To facilitate result interpretation and characterize microstructure evolution along the material flow direction, samples were grouped based on the zones outlined in *Figure 2* (gate, center, and overflow). The decrease in the area fraction of ESCs from the gate to the overflow as well as from the core to the skin layer can be seen in *Figure 6*. The former is attributed to an increasing solid fraction in the injected material, originating from ESCs accumulating towards the rear end of the shot sleeve, near the plunger face [7]. The latter is a consequence of ESC migration towards the centerline during injection. This migration is believed to result from Stoke's and Marangoni's motions developing in the nonuniform gravity and temperature fields within the highly constrained flow of material [13]. The combined influence of these mechanisms leads to a notable reduction in area fraction within the skin layer. In the current characterization, the skin layer regions in the gate, center, and overflow zones exhibit respective average ESC area fractions of 4.1%, 1.4%, and 1.1%. This finding suggests a potential variation of up to 74% in ESC area fraction within the skin layer of the plate.

Regarding the average individual crystal size distribution of the ESCs, *Figure 6(b)* reveals that ESC sizes range from 206 $\mu m^2$ to 879 $\mu m^2$, with no discernible difference between zones and regions. This consistency is coherent with the understanding that ESC modification arises from the intense shear in the runner and gate during injection. Consequently, there is no segregation of ESCs based on size and shape, leading to the stable average ESC size observed in *Figure 6(b)*.

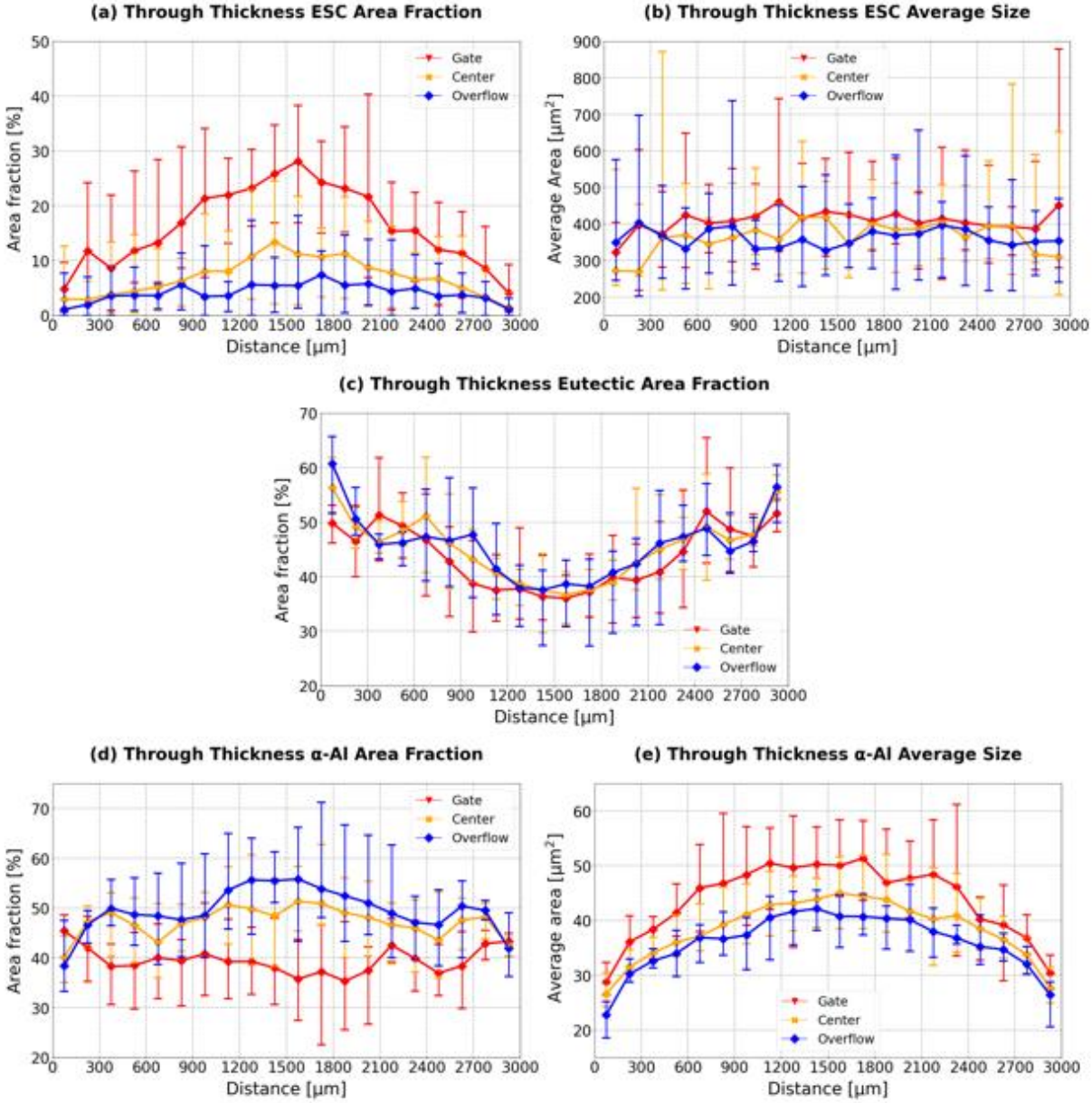


***Figure 6- Through-thickness distribution of the main constituents: (a) Area fraction of ESCs, (b) Average ESC size, (c) Eutectic area fraction, (d) α-Al area fraction and (e) Average α-Al area.***

*Figure 6(c)* presents the through-thickness distribution of eutectic for the three zones considered. The eutectic distribution within the thickness of the samples fluctuates from the skin layer to the core, but appears consistent across all zones, indicating that microstructure variation in the core results from the balance between ESCs and the α-Al phase. Segregation bands are also discernible by the eutectic plateau or peak in regions spanning from 250 to 1000 µm and 2000 to 2750 µm from the front surface. The defect band in the ejector side seems to shift toward the core as we approach the overflow, while the position of the second defect band remains stable. This observation indicates asymmetrical turbulence and material velocity levels along the centerline, leading to uneven effective pressure application on the solidifying material during the pressure intensification phase.

Finally, there is a sharp increase in the eutectic area fraction from the edge of the segregation band to the die interface in some zones. This rise peaks near the ejector surface at 49.8%, 56.3%, and 60.7% in the gate, center, and overflow zones, respectively. Conversely, the maximum eutectic area fraction near the cover surface reaches 51.2%, 55.5%, and 56.4% for the same zones. With ranges of 10.9% and 5.2% for the ejector and cover surfaces, respectively, it is evident that the process leads to asymmetrical conditions in the die cavity. These observations highlight the variability in microstructure composition within the skin layer along both the material flow and through-thickness directions.

As a consequence of the ESC and eutectic distributions, the area fraction of fine α-Al shown in *Figure 6(d)* increases along the material flow direction in the region encompassing the defect bands and the core (250 to 2750 µm), and an increase is noticeable within the skin layers (0 to 250 µm and 2750 to 3000 µm). These results are consequential to the ESCs and eutectic distribution presented in *Figures 6*. They underscore the tendency of ESCs to agglomerate in the core region, closer to the gate, as well as the substantial increase in eutectic proportion within the skin layer.

Regarding the average α-Al crystal size distribution, *Figure 6(e)* clearly demonstrates refinement in both the material flow and through-thickness directions. The average α-Al crystal size decreases from 44.3 to 40.7 $\mu m^2$ in the core and from 26.3 to 22.7 $\mu m^2$ in the skin layer.

Overall, the observations stemming from this characterization reveal significant variations in the distribution of main constituents within the part. Moreover, the constituent distribution within the skin layers throughout the plate implies a notable alteration in sub-surface microstructure composition, potentially impacting the uniformity of bending performance throughout the plate.

## SUB-SURFACE MICROSTRUCTURE CHARACTERIZATION

To better understand the impact of turbulent filling on skin layer solidification, samples from all locations depicted in *Figure 2* were analyzed to identify potential sub-surface variations within the skin layer. For clarity, in this study, the term "skin layer" refers to the microstructure situated between the segregation band and the die interface, while "sub-surface" denotes a portion of the microstructure within the skin layer in direct contact with the die interface. Consequently, a "sub-surface variant" denotes any recurring sub-surface variation in the microstructure that may arise from fluctuations in local flow or thermal conditions.

Following the through-thickness microstructure analysis of the specimens, it was determined that the edge of the segregation band is situated approximately 250 µm from the die interface. Consequently, the sub-surface characterization was conducted within the first 300 µm to capture the constituent distribution within the skin layer region. *Figure 7* illustrates representative examples of the various sub-surface variants and their respective locations, all observed within a single plate.

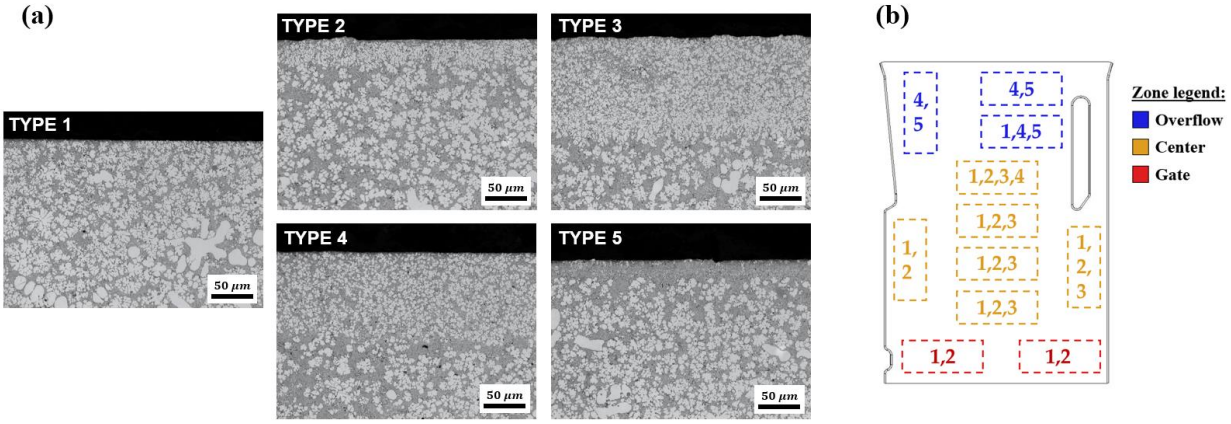


***Figure 7- Representative sub-surface microstructure variants observed within a single HPVDC Aural™-2: (a) variants micrographs and (b) variants typically observed at each of the test locations on the ejector and cover faces.***

The sub-surface variant type 1 (*Figure 8*) serves as the reference for absence of sub-surface variation, given its consistent microstructure throughout the entire skin layer. This variant is the most prevalent and has been observed in all locations of the plate except those close to the overflow. According to current understanding, this variant solidifies in zones of direct impingement or high turbulence, where the flow of material applies significant pressure on the die surface during filling. Strong impingement has been observed to limit the formation of a solidified layer or even prevent solidification at the interface altogether [9,10]. The area fraction of the main constituents for this type of sub-surface variant varies accordingly with the results presented in *Figures 6* and *Figure 8*.

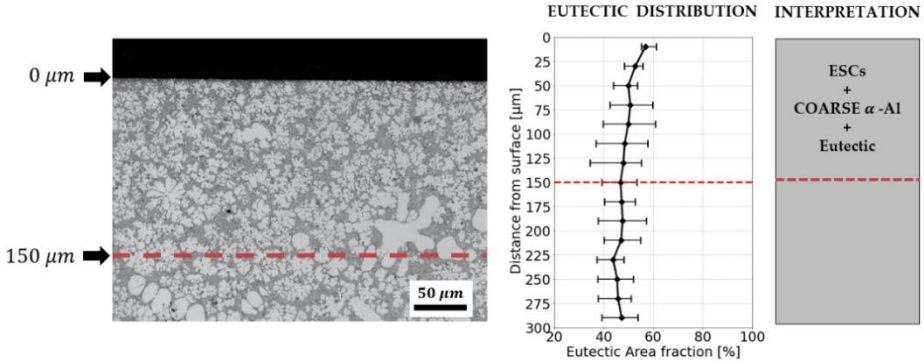


***Figure 8- Representation and interpretation of the sub-surface variant type 1.***

The sub-surface variant type 2 (*Figure 9*) is distinguished by an accumulation of α-Al at the die interface. It is typically observed in zones of moderate impingement. The α-Al density at the interface and the presence of a minor defect band suggests the occurrence of dilatant shear banding. This formation could be attributed to the impact of pressure intensification on a solid network with low solid fraction, which develops in moderate impingement zones during injection.

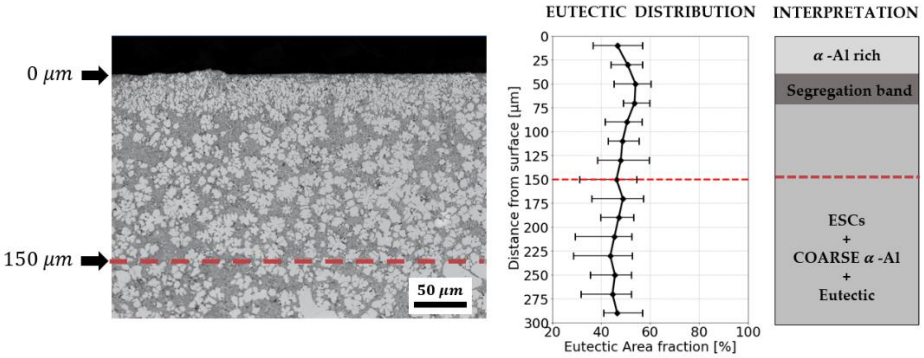


***Figure 9- Representation and interpretation of the sub-surface variant type 2.***

The sub-surface variant Type 4 (*Figure 10*) exhibits a relatively thick layer of refined α-Al phase and eutectic followed by a minor segregation band. The initiation of the refined layer from the die interface suggests a variation in thermal conditions that fosters nucleation and solidification at specific locations within the plate. Drawing from the impingement hypothesis proposed by Chen [9], this sub-surface variant could solidify in zones of low impingement. Under such conditions, a refined and cohesive solid network may form on the surface prior to the pressure intensification phase, thereby resulting in the presence of a minor segregation band between the sub-surface variant and the bulk of the skin layer.

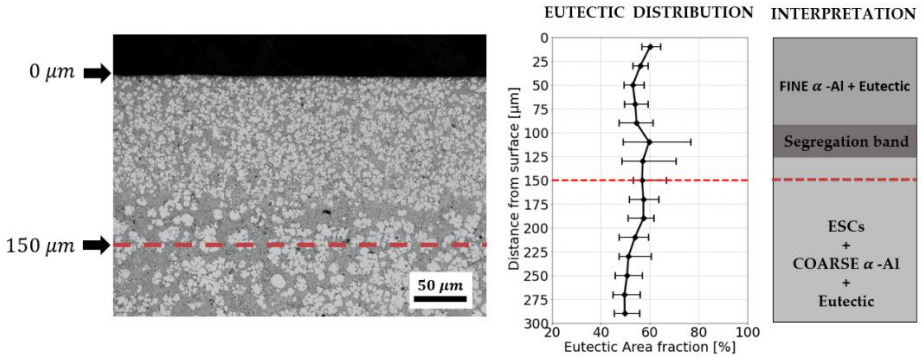


***Figure 10- Representation and interpretation of the sub-surface variant type 4.***

The sub-surface variant type 3 (*Figure 11*) combines characteristics observed in types 2 and 4, featuring a refined layer of α-Al followed by an accumulation of coarser α-Al crystals. Notably, in samples where this sub-surface variant was observed, the refined layer consistently lies between the die interface and the accumulation of α-Al crystals. This observation supports the notion that the refined layer at the interface solidifies prior to pressure intensification. Moreover, the locations where sub-surface variants 3 and 4 were observed suggest that α-Al is more likely to form toward the gate or high α-Al area fraction zones (*Figure 7(b)*).

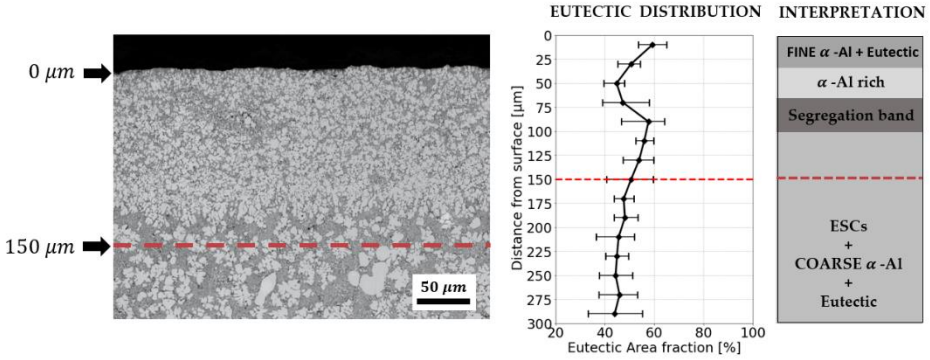


***Figure 11- Representation and interpretation of the sub-surface variant type 3.***

Finally, type 5 (*Figure 12*) is characterized by a relatively thin layer of almost pure eutectic at the die interface. Regarding its location within the plate, this variant has only been observed in samples near the overflow (*Figure 2*, I and K). It is likely a consequence of inadequate liquid feeding during the latter stages of injection in zones where solidification shrinkage pulls the solid away from the die interface. Subsequently, as the pressure intensification phase begins, dilatant shear bending develops between the solidifying material and the die surface, promoting the segregation of solute-rich material at the interface.

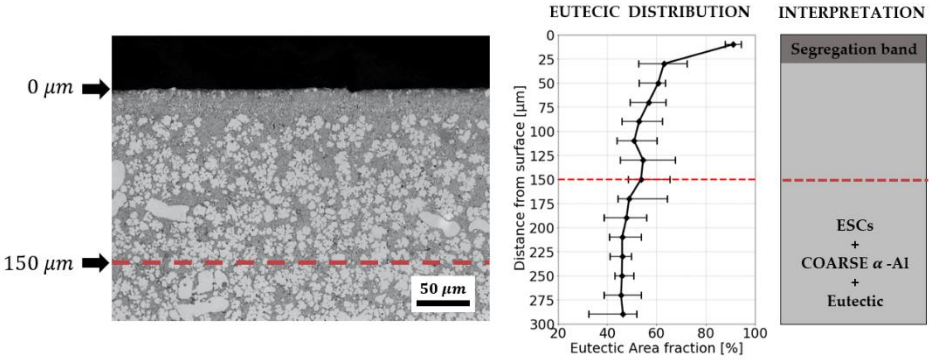


***Figure 12- Representation and interpretation of the sub-surface variant type 5.***

The microstructure within the skin layer therefore exhibits significant variation in terms of constituent area fraction and structural organization. Taking into account the findings of this study and those observed by Otarawanna et al. [17], it appears that sub-surface microstructure variations are strongly correlated with the level of impingement of the material flow (or turbulence level) and the role of dilatant shear in the segregation of the liquid phase. Moreover, it is noteworthy that the variation within the skin layer seems to be confined within the first 150 µm from the surface. In the eutectic distributions presented in *Figures 8-12*, the standard deviation within the first 150 µm is 2.16 times higher than in the rest of the skin layer. Based on the microstructure characterization conducted in this study, it is apparent that even geometrically simple HPDC parts are prone to significant local microstructure alterations within the skin layer.

## VDA BENDING RESULTS ANALYSIS

These metallographic observations are particularly intriguing when considering bending performances, as the sub-surface microstructure is believed to have the most significant influence on this test. *Figure 13* presents VDA bending results grouped by zone for samples from all locations outlined in *Figure 2*.

For the ejector surface (*Figure 13(a)*), it is evident that bending performance improves along the material flow direction, as both the bending angle and the maximum load increase from the gate to the overflow. However, the results for the cover surface are more diffuse, with less clear distinctions between the zones (*Figure 13(b)*).

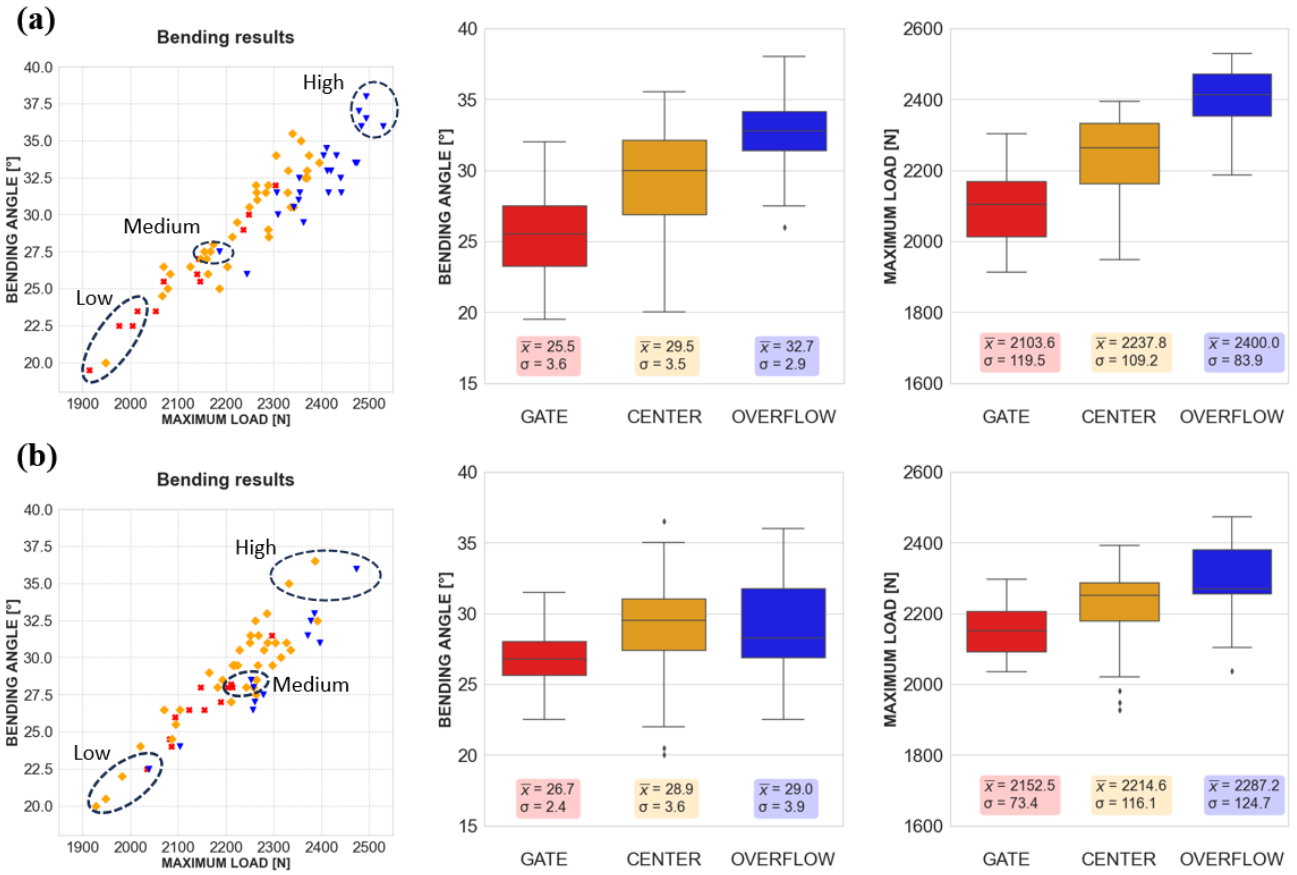


***Figure 13- VDA bending results from specimen in all considered location: (a) show the performance within the ejector surface and (b) the cover surface.***

In an effort to evaluate the impact of sub-surface microstructure variations on bending results, we have identified three subsets of bent samples based on their bending performances (low, medium, high) for visual assessment. *Figure 14* presents representative micrographs for all three performance groups on both surfaces.

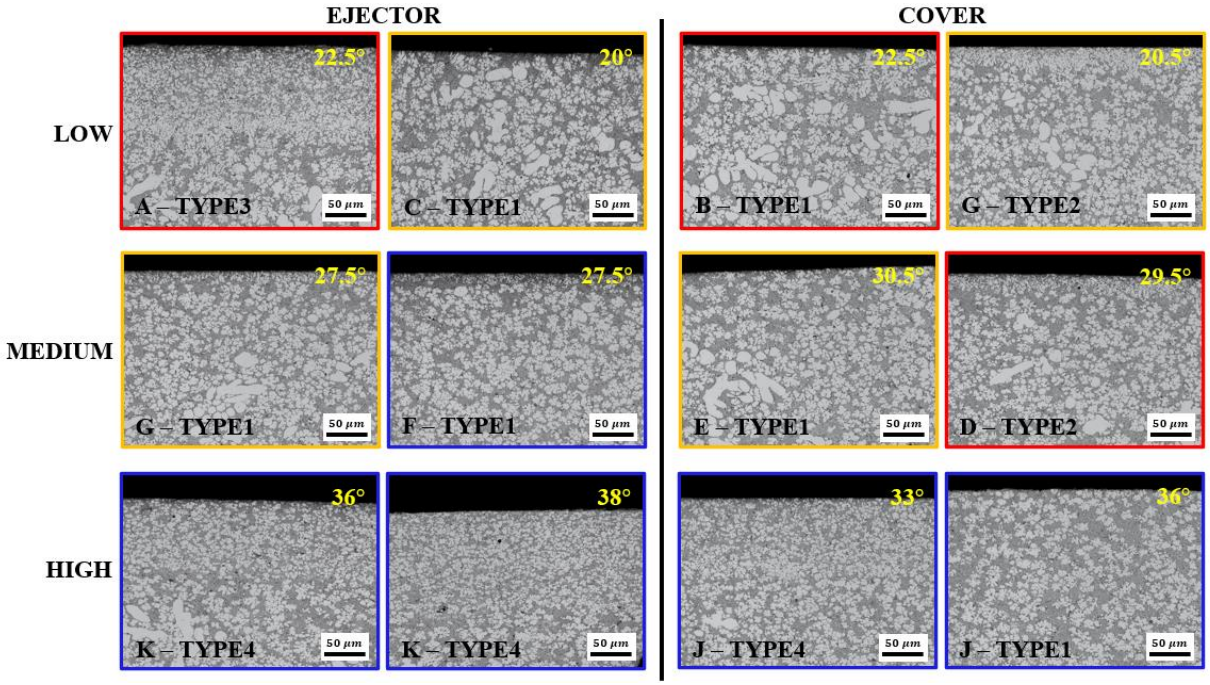


***Figure 14- Representative sub-surface microstructure for all performance groups: (a) show variants observed at the ejector surface interface and (b) the cover surface interface.***

Optical microscopy observations have revealed that most lower and medium performance specimens exhibit an absence of sub-surface variation (type 1), making it challenging to distinguish between the two groups. However, it has been noted that some low-performance samples from the back surface display sub-surface variants 2 and 3 (*Figure 9* and *Figure 11*). Upon examining the micrographs presented in *Figure 15*, it appears that these types of sub-surface variants (type 2 and 3) are detrimental to bending performance. Metallographs in *Figure 15* also show lamination type of defects at the surface, which likely contributed to degraded bending performance. The propagation of cracks through the weak plane between the refined layer and the α-Al accumulation aligns with observations regarding the solidification sequence of the different layers. Furthermore, cracks originating from the α-Al-rich layer suggest that the compacted crystal structure is conducive to crack initiation.

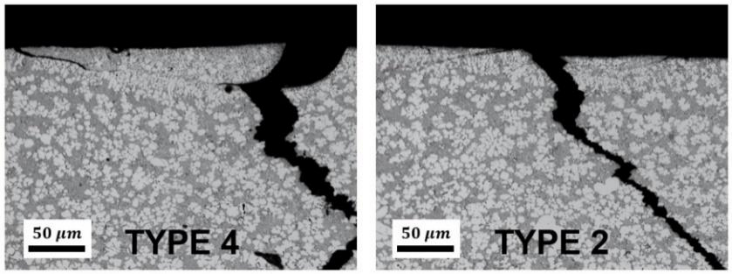


***Figure 15- Micrograph showing the detrimental effect of the sub-surface variants 2 and 4 on crack propagation during VDA bending test.***

Many of the high-performance samples from the front surface exhibit a consistent sub-surface variation characterized by a refined α-Al layer mixed with eutectic (*Figure 10* – type 4). Conversely, high-performance specimens from the back surface display either a layer of refined α-Al or an absence of sub-surface variant. Since an absence of sub-surface variation has been observed in specimens from all performance groups, it is likely that the size and area fraction of the main constituents are more significant factors than the mere presence of a sub-surface variant.

The subjective nature of identifying sub-surface microstructure variants alone is insufficient to fully explain the observed variations in bending performances across the plate. Therefore, in an effort to objectively characterize the sub-surface microstructure of each subset, the eutectic area fraction, average α-Al crystal area, and ESC area fraction have been calculated within the first 150 μm of each sample. Results from this analysis are presented in *Figure 16*, clearly illustrating a distinction between the performance groups. The low-performance group is characterized by a significant decline in eutectic content, a coarser α-Al phase, and a higher proportion of ESCs. Conversely, the medium-performance group exhibits a more stable eutectic content, a slightly finer α-Al phase, and considerably fewer ESCs.

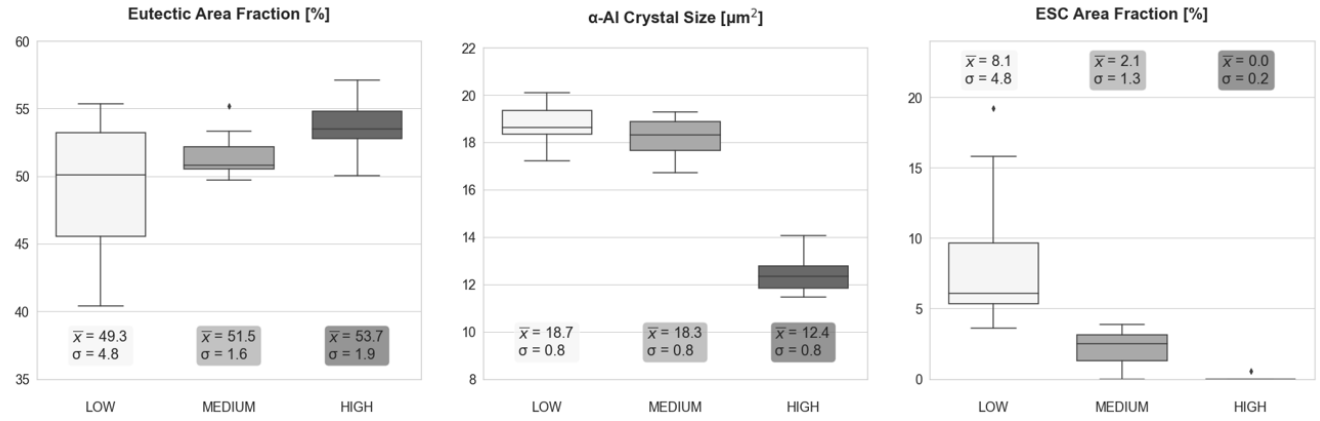


***Figure 16- Main constituents' distribution within the first 150 μm from the interface of both surfaces: (a) the eutectic area fraction, (b) the α-Al average crystal area, and (c) the area fraction of ESCs.***

All in all, the distinction between low and medium performance samples in terms of bending angle can be primarily attributed to the ESC content within the skin layer and the presence of detrimental sub-surface variants. Conversely, high-performance samples are characterized by a pronounced refinement of the α-Al phase mixed with eutectic (type 4) and an absence of ESCs. These findings suggest that the average size of α-Al crystals and the distribution of ESCs within the skin layer are the most influential factors affecting the homogeneity of bending performance across the plate.

## CONCLUSION

In this study, local variations within the as-cast microstructure of an HPVDC plate were investigated with specific focus on the near-surface regions. The aim was to characterize possible sub-surface microstructure variants within a single plate and assess their influence on local bending performances.

While the specimens were simple flat plates, the process still generated a variety of near-surface characteristics. The following conclusions can be drawn on the influence of sub-surface variants on bending performances:

- The presence of ESCs in the skin layer negatively impacts local bending performance.
- Sub-surface variants with a refined layer of α-Al mixed with eutectic contribute to enhanced bending performance.
- The α-Al rich layer has detrimental consequences, promoting crack initiation at the surface and within the sub-surface by creating a weak plane between the solid network present at the interface.
- At a given location on the part, a subset of different sub-surface variants can be found in successive individual parts, highlighting the stochastic factors in die filling.

Based on these findings, sub-surface characteristics plays a clear role on the bending performances of HPVDC thin-walled components. As evidenced in the literature, more complex geometries could lead to a wider range of microstructures as melt impact angles on the die cavity vary and the flow pattern becomes more intricate. Continued investigation on more representative prototypes or industrial scale specimens could refine our understanding of the mechanisms at play in microstructure formation. This knowledge could allow us to identify factors that could help predict, and eventually control, variations within a single component at the design and process setup stages.

## ACKNOWLEDGMENTS

This work was carried out as part of a project supported by the NRC's METALTec industrial research and development group members and sponsors, as well as the NRC's National Program Office (Grant # AM-126-1). The authors wish to acknowledge the contributions of the NRC team who participated in this study, Siyu Tu, Alexandre Morin and Keven Lepage-Potvin, as well as those from the UQAC team, Ali Elashery and Zhixing Chen.

## REFERENCES

1. G. G. Wang et J. Weiler, "Recent developments in high-pressure die-cast magnesium alloys for automotive and future applications," Journal of Magnesium and Alloys, vol. 11, no. 1, pp. 78-87, 2023.
2. M. Guo, M. Sun, J. Huang, et S. Pang, "A Comparative Study on the Microstructures and Mechanical Properties of Al-10Si-0.5 Mg Alloys Prepared under Different Conditions. Metals (Basel) 2022; 12."
3. D. S. Cantú-Fernández, J. J. Taha-Tijerina, A. González, P. G. Hernández, et B. Quinn, "Mechanical Properties of a Structural Component Processed in High-Pressure Die Casting (HPDC) with a Non-Heat-Treated Aluminum Alloy," Metals, vol. 14, no. 3, p. 369, 2024.
4. Q. Sun et al., "Formation mechanism of the microstructural heterogeneity in a die-cast Al-Mg-Si alloy and its effect on mechanical properties," Materials Characterization, p. 114004, 2024.
5. G. Timelli et A. Fabrizi, "The Effects of Microstructure Heterogeneities and Casting Defects on the Mechanical Properties of High-Pressure Die-Cast AlSi9Cu3(Fe) Alloys," Metallurgical and Materials Transactions A: Physical Metallurgy and Materials Science, vol. 45, no. 12, pp. 5486-5498, 2014. doi: 10.1007/s11661-014-2515-7.
6. H. Zheng, Y. Jiang, F. Liu, et H. Zhao, "Microstructure heterogeneity optimization of HPDC Al-Si-Mg-Cu alloys by modifying the characteristic of externally solidified crystals," Journal of Alloys and Compounds, vol. 976, Article 173167, 2024. doi: 10.1016/j.jallcom.2023.173167.
7. H. Laukli, O. Lohne, S. Sannes, H. Gjestland, et L. Arnberg, "Grain size distribution in a complex AM60 magnesium alloy die casting," *International Journal of Cast Metals Research*, vol. 16, no. 6, pp. 515-521, 2003.
8. S. Otarawanna, C. Gourlay, H. Laukli, et A. Dahle, "Microstructure formation in AlSi4MgMn and AlMg5Si2Mn high-pressure die castings," *Metallurgical and Materials Transactions A*, vol. 40, pp. 1645-1659, 2009.
9. Z. Chen, "Skin solidification during high pressure die casting of Al–11Si–2Cu–1Fe alloy," *Materials Science and Engineering: A*, vol. 348, no. 1-2, pp. 145-153, 2003.
10. S. Otarawanna, C. Gourlay, H. Laukli, et A. Dahle, "Formation of the surface layer in hypoeutectic Al-alloy high-pressure die castings," *Materials Chemistry and Physics*, vol. 130, no. 1-2, pp. 251-258, 2011.
11. Z. Yuan, Z. Guo, et S. Xiong, "Skin layer of A380 aluminium alloy die castings and its blistering during solution treatment," Journal *of Materials Science & Technology*, vol. 35, no. 9, pp. 1906-1916, 2019.
12. C. Gourlay, H. Laukli, et A. Dahle, "Defect band characteristics in Mg-Al and Al-Si high-pressure die castings," *Metallurgical and Materials Transactions A*, vol. 38, pp. 1833-1844, 2007.

13. S. Ji, Y. Wang, D. Watson, et Z. Fan, "Microstructural evolution and solidification behavior of Al-Mg-Si alloy in high-pressure die casting," *Metallurgical and Materials Transactions A*, vol. 44, pp. 3185-3197, 2013.
14. W. Yu, C. Ma, Y. Ma, et S. Xiong, "Correlation of 3D defect-band morphologies and mechanical properties in high pressure die casting magnesium alloy," *Journal of Materials Processing Technology*, vol. 288, p. 116853, 2021.
15. V.d. Automobilindustrie, VDA 238-100 Plate bending test for metallic materials, 2010.
16. A. Gariépy, "Weldability of HPVDC structural alloy: impact of surface and core characteristics," presented at NADCA, 2023.
17. S. Otarawanna, H. Laukli, C. Gourlay, et A. Dahle, "Feeding mechanisms in high-pressure die castings," Metallurgical and Materials transactions A, vol. 41, pp. 1836-1846, 2010.